

A proposal to construct the dark-matter-only counterpart of the observed Universe combining weak lensing and baryon censuses

Shuren Zhou^{1,2,3,4*} and Pengjie Zhang^{2,1,3,4†}

¹ *Tsung-Dao Lee Institute, Shanghai Jiao Tong University, Shanghai 201210, China*

² *School of Physics and Astronomy, Shanghai Jiao Tong University, Shanghai 200240, China*

³ *State Key Laboratory of Dark Matter Physics, Shanghai 200240, China*

⁴ *Key Laboratory for Particle Astrophysics and Cosmology (MOE)/Shanghai Key Laboratory for Particle Physics and Cosmology, Shanghai 200240, China*

(Dated: November 17, 2025)

Baryonic effects such as AGN feedback can significantly impact the matter clustering, are harder to model from first principles, and emerge as a severe limiting factor in weak lensing cosmology. To tackle this issue, we propose a generic relation of mapping the observed matter clustering to its counterpart in a dark-matter-only universe. We verify this relation to be accurate at better than 1% level at $k < 1h/\text{Mpc}$ and $z \in [0, 3]$ in both TNG and Illustris simulations, demonstrating its model-independence to the underlying baryonic physics. Implementing this relation in observations will be made possible by the specifically designed cross-correlation statistics and baryon census (ionized diffuse gas through localized fast radio bursts, stellar mass through galaxy surveys, and neutral hydrogen through 21cm mapping). It is capable of correcting the baryonic effect not only in the matter power spectrum, but also at the field level, as demonstrated by tests on the scattering transform statistics. This approach paves the way for constructing the dark-matter-only counterpart of the observed Universe, establishing an ideal cosmological laboratory for probing the dark universe.

Introduction.— Forthcoming surveys will measure weak gravitational lensing and therefore the matter clustering with unprecedented precision, shedding light on fundamental cosmological physics such as dark energy and gravity. However, the scientific returns are limited by baryonic effects such as AGN/SN feedback and gas cooling. These processes alter the matter clustering in complicated ways (cold gas, [1]; hot gas, [2]; hydrodynamical simulations [3–6]) and can reach $\sim 10\%$ at $k = 1h/\text{Mpc}$. Given the expected $S/N \gtrsim 400$ of the weak lensing measurements by LSST [7] and CSST [8], this baryonic effect will become a leading systematic error. It also significantly impacts other large-scale structure probes.

One potential solution for baryonic effects is cosmological hydrodynamical simulations, which incorporate baryon physics in subgrid [6, 9–16]. But due to the lack of a first-principle treatment for baryon processes, different simulations yield diverse results [17, 18], and exhibit varying degrees of tension with observations [19–21]. Alternative strategies attempt to post-process dark-matter-only (DMO) simulations to mimic baryonic effects phenomenologically [22–25], which require observational calibrations and induce model/parameterization dependence. Observations of the Sunyaev-Zel’dovich effects [19, 26, 27], X-ray emission [20, 21, 28, 29], and various baryon censuses [30–35] have significantly advanced our understanding of baryonic processes. However, each of these probes is sensitive to baryons in specific forms and on limited scales. Either inferences using a single probe or joint fits of multiple probes inevitably rely on modeling baryons, whose uncertainties would eventually propagate to the cosmological inferences.

Given the stringent requirements of probing fundamental physics with weak lensing, it is imperative to develop

alternative methods to correct baryonic effects. In this paper, we propose an observation-based method to accurately correct baryonic effects, independent of modeling baryonic physics. As this approach is carried out at the field level, it essentially constructs a DMO universe, the counterpart of the observed Universe.

A generic relation to correct baryonic effects.— The complete treatment of baryonic effects requires a direct relation between the matter clustering of δ_m and its counterpart of δ_{DMO} in a hypothetical DMO universe, where the former is in principle an observable and the latter is fully predicted by gravity theory. $\delta_m = \Omega_m^{-1}(\Omega_c \delta_c + \Omega_b \delta_b)$, where δ_c/δ_b is the cold dark matter/baryon overdensity in the real universe. Although δ_b can deviate significantly from δ_c and δ_{DMO} , the difference in δ_c and δ_{DMO} should be much smaller because of $\Omega_b \ll \Omega_c$.

To establish the δ_m - δ_{DMO} relation, we assume that **(I)** *baryonic effects do not alter the phase of the matter overdensity relative to its DMO counterpart*. If so, the mapping between δ_{DMO} and δ_m is fully determined by a transfer function $\mathcal{T}(k)$ in Fourier space, with $k = |\mathbf{k}|$.

$$\delta_{\text{DMO}}(\mathbf{k}) = \mathcal{T}(k) \delta_m(\mathbf{k}) . \quad (1)$$

Under this assumption, \mathcal{T} fully encapsulates the baryonic effects on the matter clustering.

To solve for \mathcal{T} , we further assume that **(II)** *the δ_{DMO} field can be approximated by the cold dark matter overdensity field δ_c* . It leads to

$$\delta_{\text{DMO}} \simeq \delta_c = (\Omega_m \delta_m - \Omega_b \delta_b) / \Omega_c . \quad (2)$$

Baryons can be categorized into three major components: ionized diffuse gas, neutral gas, and stellar content. All

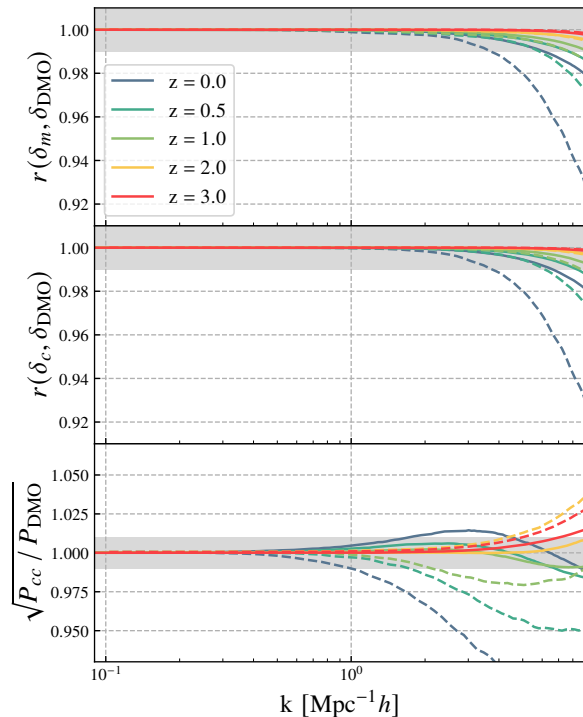


FIG. 1. Validation of the assumptions (I) and (II) using TNG300-1 (solid lines) and Illustris-1 (dashed lines) simulations. The shaded regions mark the $\pm 1\%$ deviation. *Top*: Cross-correlation coefficients between total matter overdensity δ_m in hydrodynamical simulation and its DMO counterpart δ_{DMO} . *Middle*: Cross-correlation coefficients between cold dark matter overdensity δ_c and δ_{DMO} . *Bottom*: Ratio of the power spectrum P_{cc} of δ_c to P_{DMO} of δ_{DMO} . Despite the different subgrid physics implemented in two simulations, both confirm assumption (I) to be $< 0.1\%$ accuracy and assumption (II) to be $< 1\%$ accuracy at scales $k < 1 h/\text{Mpc}$.

these components are direct observables in principle, and the total baryon overdensity is thereby [36]

$$\delta_b = \frac{1 + \eta}{1 + \frac{1}{2}\eta} f_e \delta_e + f_* \delta_* + (1 + \eta) f_{\text{HI}} \delta_{\text{HI}}. \quad (3)$$

Here, $f_* \equiv \Omega_*/\Omega_b$ and $f_{\text{HI}} \equiv \Omega_{\text{HI}}/\Omega_b$ are the baryon mass fraction of the species. $\eta = X_{\text{H}}/X_{\text{He}}$, where $X_{\text{H}} \simeq 0.76$ and $X_{\text{He}} \simeq 0.24$ are mass abundances of hydrogen and helium elements. The ionized electrons overdensity δ_e is probed by the dispersion measure of fast radio bursts (FRBs), which is the major contribution in the baryon budget of fraction $f_e \equiv f_{\text{HII}} + \frac{1}{2} f_{\text{HeII}} \sim 0.8$. The subdominant components are stars and stellar remnants overdensity δ_* of fraction $f_* \sim 5\%$, and neutral hydrogen overdensity δ_{HI} of fraction $f_{\text{HI}} \sim 5\%$ traced by 21cm lines [37]. Substituting Eq. (2)&(3) into Eq. (1), we obtain

$$\hat{\mathcal{T}}(k) = \frac{\Omega_m}{\Omega_c} - \frac{\Omega_b}{\Omega_c} \left[\frac{1 + \eta}{1 + \frac{1}{2}\eta} f_e b_e + f_* b_* + (1 + \eta) f_{\text{HI}} b_{\text{HI}} \right]. \quad (4)$$

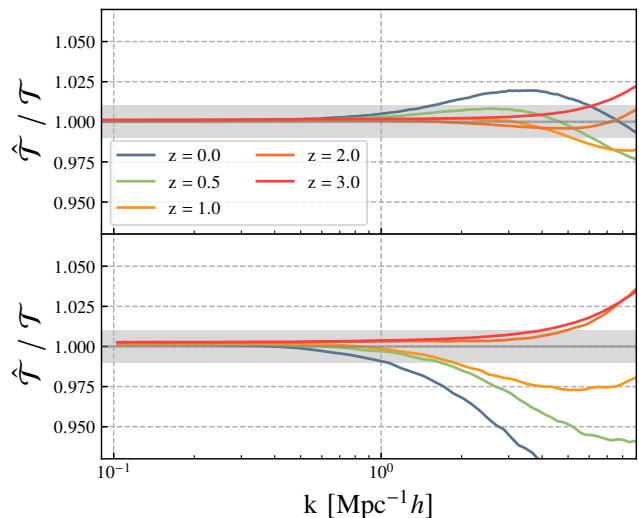


FIG. 2. Validation of the key relation Eq. (4). We show the ratio of the estimated transfer function $\hat{\mathcal{T}}$ to the ground truth $\mathcal{T} = \sqrt{P_{\text{DMO}}/P_{mm}}$, measured in TNG300-1 (top) and Illustris-1 (bottom) simulations. Luminous subhalos are identified as galaxies and cross-correlated with the ionized electrons (δ_e), stars + black holes (δ_*), and neutral hydrogen (δ_{HI}) to measure $\{f_e b_e, f_* b_*, f_{\text{HI}} b_{\text{HI}}\}$, and hence $\hat{\mathcal{T}}$. These results indicate that $\hat{\mathcal{T}}$ agrees with the true \mathcal{T} within $< 1\%$ accuracy on scales $k < 1 h/\text{Mpc}$ across redshift range $0 < z < 3$, regardless of the strength of baryonic effects.

Here b_i denotes the scale-dependent baryon bias of the i species.

The relations of Eq. (4) together with Eq. (1) are the major results of this paper. It maps δ_m in the real universe to its counterpart δ_{DMO} in a hypothetical DMO universe, using $\hat{\mathcal{T}}$ obtained from observational baryon censuses. It not only corrects baryonic effects in the matter power spectrum ($P_{mm} \rightarrow \hat{\mathcal{T}}^2 P_{mm}$), but also at the field level ($\delta_m(\mathbf{k}) \rightarrow \hat{\mathcal{T}}(k) \delta_m(\mathbf{k})$). Next, we validate these relations in hydrodynamical simulations, before we discuss their implementation in observations.

Simulation validations.— We validate the assumption (I), (II) and Eq. (4) using hydrodynamical simulations TNG300-1 [39–43], Illustris-1 [44–47], and their DMO counterparts. To accommodate the observational implementation discussed later, the baryon bias b_i in Eq. (4) is measured by the cross-correlations with galaxy overdensity δ_g , i.e., $b_i(k) \equiv P_{gi}(k)/P_{gm}(k)$, where the galaxy samples is chosen as all luminous subhalos in simulations. The validity of the assumption (I) is quantified by the cross-correlation coefficient $r(\delta_m, \delta_{\text{DMO}})$, shown in Fig. 1. At the benchmark scale of $k = 1 h/\text{Mpc}$, the TNG300-1 results show no visible deviation, and the largest deviation in Illustris-1 occurs at $z = 0$ where $1 - r \simeq 0.1\%$. In Ref. [17], the measurements from thousands of hydrodynamical simulations present a more comprehensive justification of the assumption (I). In the

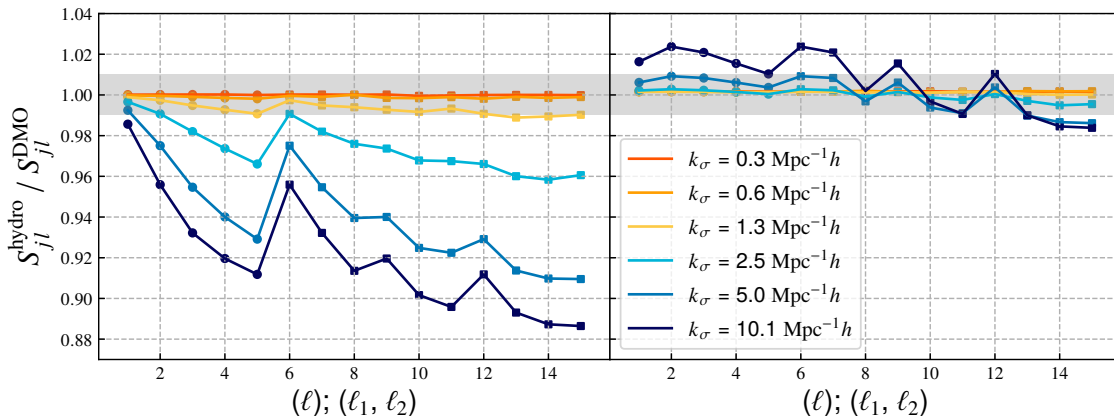


FIG. 3. Validation of the field-level correction capability. We take the scattering transform as an example, which contains higher-order correlations and phase information. *Left*: Ratio of coefficients from δ_m in Illustris-1 simulation at $z = 0.5$ to its DMO counterpart δ_{DMO} . *Right*: Ratio of coefficients from those with the \mathcal{T} correction, $\hat{\delta}_{\text{DMO}}(\mathbf{x}) = \hat{\mathcal{T}} * \delta_m(\mathbf{x})$, to δ_{DMO} . We measure the first two order coefficients, S_{jl} and $S_{j_1 l_1; j_2 l_2}$, and set $j_1 = j_2$ & $l_1 > l_2$ in $S_{j_1 l_1; j_2 l_2}$ to reduce data size [38]. In each panel, different lines represent spatial index $j \in \{0, 1, 2, 3, 4, 5\}$, corresponding to the filter size $k_\sigma = 2\pi/\sigma_j$ in Fourier space. The horizontal ordinates represent angular indexes $\ell \in \{0, 1, 2, 3, 4\}$, sorted as $\{\ell = 0, \ell = 1, \dots, (\ell_1, \ell_2) = (1, 0), (\ell_1, \ell_2) = (2, 0), \dots\}$. The accurate removal of baryonic effects down to resolution $k_\sigma \lesssim 2 h/\text{Mpc}$ demonstrates the effectiveness of the $\hat{\mathcal{T}}$ correction at the field-level.

appendix, we provide a Lagrangian-space demonstration for the two opposite behaviors of matter clustering: the insensitivity of the phase and the sensitivity of the amplitude to baryonic effects.

To validate the assumption (II), we measure $r(\delta_c, \delta_{\text{DMO}})$ and $\sqrt{P_{cc}/P_{\text{DMO}}}$ to quantify the phase and amplitude differences between $\delta_c(\mathbf{k})$ and $\delta_{\text{DMO}}(\mathbf{k})$ respectively (Fig. 1). The phases are nearly identical, with $1 - r < 0.1\%$ at $k < 1 h/\text{Mpc}$ for both simulations. The amplitudes deviate more significantly, particularly in Illustris-1. This larger discrepancy arises from the stronger AGN feedback implemented in Illustris-1, which substantially modifies the matter distribution, especially baryons residing in halos [20, 46]. Nevertheless, even under such aggressive feedback, the maximum deviation remains below $\sim 1\%$ at $z = 0$ around $k \sim 1 h/\text{Mpc}$, confirming the robustness of the assumption (II) on scales $k \lesssim 1 h/\text{Mpc}$. It is a consequence of $\Omega_c \gg \Omega_b$ and the delayed response of cold dark matter clustering to baryon processes, as their interaction occurs solely through gravitational potential changes, rather than through direct feedback mechanisms.

The validations of these assumptions already ensure the robustness of the $\hat{\mathcal{T}}$ derivation. Furthermore, direct measurements in simulations confirm $\hat{\mathcal{T}} = \mathcal{T}$ within 1% accuracy on scales $k < 1 h/\text{Mpc}$ (Fig. 2) and $z \in [0, 3]$, despite significantly different feedback strengths adopted in TNG300-1 and Illustris-1. Here $\mathcal{T} = \sqrt{P_{\text{DMO}}/P_{mm}}$ is the ground truth. It explicitly indicates that the baryonic effect on the matter power spectrum can be corrected accurately at $k < 1 h/\text{Mpc}$. On smaller scales $k = 1 \sim 10 h/\text{Mpc}$, deviations increase to $\sim 2\%$ in TNG300-1 and

$\sim 8\%$ in Illustris-1 at $z = 0$. The primary source of these deviations is the assumption (II), since baryons indeed modify the clustering amplitude of cold dark matter on Mpc and smaller scales (Fig. 1).

We emphasize that by design, our method removes baryonic effects at the field level. Therefore, baryonic effects in other summarized statistics are removed as well. To illustrate, we take the scattering transform [38, 48–50] as an example of beyond 2-point statistics. We adopt the Gaussian-Legendre wavelet filter to extract features of the 3D isotropic field, $\psi_{jl}(\mathbf{x}) = \exp[-r^2/(2\sigma_j^2)] r^l P_l(\cos\theta)$. The Gaussian function determines the spatial correlation by scaling $\sigma_j \equiv \sigma/2^j$, while the Legendre polynomials P_l determine the angular correlation. The scattering transform coefficients of the stochastic field, e.g., $I_0 = \delta_m(\mathbf{x})$, are obtained following,

$$\begin{aligned} S_{jl} &= \langle I_{jl} \rangle_{\mathbf{x}} = \langle |I_0 * \psi_{jl}| \rangle_{\mathbf{x}}, \\ S_{j_1 l_1; j_2 l_2} &= \langle I_{j_1 l_1; j_2 l_2} \rangle_{\mathbf{x}} = \langle |I_0 * \psi_{j_1 l_1} * \psi_{j_2 l_2}| \rangle_{\mathbf{x}}. \end{aligned} \quad (5)$$

Here, $*$ denotes the convolution operator, and $\langle \dots \rangle_{\mathbf{x}}$ indicates averaging over all real-space pixels. The non-linear operations in the scattering transform enable the extraction of higher-order correlations and phase information.

In Fig. 3, we present the Illustris-1 results at $z = 0.5$, in which Baryonic effects suppress the scattering coefficients up to $\sim 10\%$. After applying the transfer function to remap the matter field, i.e., $\hat{\delta}_{\text{DMO}}(\mathbf{x}) = \hat{\mathcal{T}} * \delta_m(\mathbf{x})$ by Eq. (1)&(4), the scattering coefficients of the reconstructed field $\hat{\delta}_{\text{DMO}}$ agree with those measured in δ_{DMO} , down to resolution of $k_\sigma \equiv 2\pi/\sigma_j \lesssim 2 h/\text{Mpc}$. For

$k_\sigma \gtrsim 5 h/\text{Mpc}$, the scattering coefficients incorporate the small-scale modes that are not fully recovered by $\hat{\mathcal{T}}$, resulting in increasing deviations with larger k_σ . It is consistent with the accuracy of $\hat{\mathcal{T}}$ shown in Fig. 2. Nevertheless, even for $k_\sigma \simeq 10 h/\text{Mpc}$, the deviation is smaller than 2%. This example demonstrates that $\hat{\mathcal{T}}$ corrects baryonic impacts on non-Gaussian statistics/phase, validating its capability to remove baryonic effects at the field-level.

Observational implementation.— In observations, the clustering of matter and baryons is often measured from 2D projected fields on the sky. For weak lensing, we can first conduct 3D lensing to reconstruct the 3D δ_m fields (with poor redshift resolution) [51–53], and then average over the chosen redshift range to obtain the projected δ_m field. Straightforwardly, relations of Eqs. (1)–(4) can be translated from Fourier space of \mathbf{k} to harmonic space of ℓ , namely,

$$\mathbf{k} \rightarrow \ell, \mathcal{T}(k) \rightarrow \mathcal{T}(\ell), b_i(k) \rightarrow b_i(\ell), \dots \quad (6)$$

Since the related 2D quantities are the 3D ones averaged over the corresponding redshifts and scales, the relation in 2D must hold as well. Now the transfer function $\mathcal{T}(\ell)$ maps the observed 2D matter clustering in weak lensing to its DMO counterpart.

To measure $\hat{\mathcal{T}}$ in observations, we combine 5 probes $X \in \{\Delta_g, \kappa, \mathcal{D}, \Sigma_*, T_b\}$: the galaxy overdensity Δ_g , weak lensing convergence κ , dispersion measure \mathcal{D} of FRBs, stellar surface density Σ_* , and surface brightness temperature T_b of 21cm lines. They are projected fields and related to the underlying 3D overdensity $Y \in \{\delta_g, \delta_m, \delta_e, \delta_*, \delta_{\text{HI}}\}$ by $X(\hat{n}) = \int Y(\hat{n}, \chi) W_X(\chi) d\chi$, where W_X is the kernel function. The auxiliary galaxy data Δ_g is crucial in extracting the redshift information of weak lensing and dispersion measure arising from the intergalactic medium, so its redshift distribution should be sufficiently narrow. The combination $f_i b_i$ in Eq. (4) is therefore measured by

$$\widehat{f_i b_i}(\ell) = \hat{\mathcal{A}}_i \frac{\hat{C}_\ell^{gX_i}}{\hat{C}_\ell^{g\kappa}}. \quad (7)$$

Here the angular power spectra C_ℓ^{AB} is defined through $\langle A_\ell B_\ell^* \rangle = \delta_{\ell\ell'}^D C_\ell^{AB}$. The normalization factor \mathcal{A}_i of the i species only relies on the cosmological parameters, and their exact expressions of $\mathcal{A}_e, \mathcal{A}_*, \mathcal{A}_{\text{HI}}$ are provided in the appendix. Utilizing the tight constraint of cosmological parameters from CMB observations [54, 55] and BAO surveys [56, 57], we can accurately determine the amplitude \mathcal{A}_i in Eq. (7) and the energy fractions Ω_i in Eq. (4), thereby fully measuring the transfer function \mathcal{T} in observations, independent of model assumptions.

Observation prospects.— Two auxiliary probes in \mathcal{T} measurement, galaxy clustering Δ_g and weak lensing κ , are being precisely measured in current galaxy surveys such as DESI [58] and Rubin [7], and further improved

by surveys like CSST [8] and MUST [59]. The limiting factors are baryon census using \mathcal{D} , Σ_* , and T_b .

The dispersion measure of FRB [60] directly probes free electrons in the ionized diffuse gas, which represents the majority of cosmic baryons [33, 35, 61]. Thus $f_e b_e$ is key in determining $\hat{\mathcal{T}}$. Its measurement utilizes cross-correlation statistics between \mathcal{D} and galaxies at lower redshifts. This naturally separates the intergalactic medium contribution from host galaxy contamination. To identify the host galaxy redshifts, FRB localization is required. Given the significant event rate [62] and advances of high angular resolution and wide field-of-view FRB surveys (e.g., DSA-2000 [63] and BURSTT [64]), a sample of $\sim 10^5$ localized FRBs is achievable. Adopting the same redshift distribution in Ref. [36] and bin size $\Delta \log \ell = 0.3$, this moderate estimate of FRB sample size in combination with a DESI-like survey already achieves cross-correlation signal-to-noise ratio $C_\ell^{g\mathcal{D}}/\sigma_{C_\ell} \sim 10$ over modes of $0.1 \sim 1 h/\text{Mpc}$. Since ionized diffuse electrons are the dominant contribution in $\hat{\mathcal{T}}$, the limited FRB sample size primarily determines the measurement accuracy of \mathcal{T} . $\delta\mathcal{T}/\mathcal{T} \sim \Omega_b/\Omega_c \delta(f_e b_e) \sim \Omega_b/\Omega_c \sigma_{C_\ell}/C_\ell^{g\mathcal{D}} \sim 0.01$, satisfying the stringent requirement of baryonic effect correction.

The contributions from stars and stellar remnants $f_* b_*$ and neutral hydrogen $f_{\text{HI}} b_{\text{HI}}$ are subdominant. Given that $f_* + f_{\text{HI}} \sim 0.1$ and $b_*, b_{\text{HI}} \gtrsim 1$, neglecting these components would introduce a systematic bias at the $\gtrsim 1\%$ level. This shift is negligible in the previous surveys, but exceeds the statistical limit in LSST-like surveys. As argued in Ref. [36] in the context of a cosmological Cavendish experiment, both $f_* b_*$ and $f_{\text{HI}} b_{\text{HI}}$ would be measured precisely with galaxy surveys and 21cm surveys. We refer the readers to Ref. [36] for a detailed discussion. Together with Ref. [36], the combination of weak lensing, galaxy surveys, and localized FRBs sheds light on both gravitational and baryonic physics.

Discussions and conclusions.— In summary, we derive a generic relation that maps the observed matter density field to its DMO counterpart. Its implementation in observations will be realized by multiple probes, including weak lensing, galaxy surveys, and localized FRBs. The relation is validated to be accurate at better than 1% level for scales $k < 1 h/\text{Mpc}$ across the redshift range $0 < z < 3$, and enables the field-level corrections of baryonic effects independent of modeling baryon physics. This will recover information in the non-linear regime obscured by baryonic physics, and significantly enhance the constraining power of weak lensing cosmology.

Nevertheless, our method implicitly assumes that only the matter field is clustered, so it does not apply in scenarios with clustered dark energy. Moreover, its observational implementation of Eq. (7) assumes that the effective gravitational constant of light propagation is $G_{\text{light}} = G$. It is consequently not applicable to modified gravity models with $G_{\text{light}} \neq G$, in which $\hat{\mathcal{T}}$ is biased

due to biased estimate $\widehat{f_i b_i} = f_i b_i (G/G_{\text{light}})$. A possible approach to break the degeneracy between G_{light} and \mathcal{T} is the cosmological Cavendish experiment proposed in Ref. [36], which employs the same data set to measure G_{light} . Since the analysis in that work is restricted to scales $k \lesssim 0.1 h/\text{Mpc}$, the measured G_{light} is immune to baryonic effects. However, a remaining concern is whether the G_{light} measured on large scales can be extrapolated to $k \sim 1 h/\text{Mpc}$ relevant for determining \mathcal{T} . Without resolving this issue, our method is restricted to Einstein's theory and modified gravity models that satisfy $G_{\text{light}} = G$, such as the $f(R)$ gravity.

During the preparation of this work, a proposal employing FRBs to null baryonic effects was published [61]. Both works use FRBs as a primary source of information on baryonic effects and demonstrate the great potential of baryon census enabled by emerging probes. Nonetheless, the two works differ in methodology, observational implementation, and performance, and are therefore complementary to each other.

Acknowledgments.— This work is supported by the National Key R&D Program of China (2023YFA1607800, 2023YFA1607801), and the Fundamental Research Funds for the Central Universities. Shuren Zhou is also supported by T.D. Lee scholarship. This work made use of the Gravity Supercomputer at the Department of Astronomy, Shanghai Jiao Tong University.

* zhoushuren@sjtu.edu.cn

† zhangpj@sjtu.edu.cn

- [1] M. White, *Astroparticle Physics* **22**, 211 (2004).
- [2] H. Zhan and L. Knox, *The Astrophysical Journal* **616**, L75 (2004).
- [3] Y. Jing, P. Zhang, W. Lin, L. Gao, and V. Springel, *The Astrophysical Journal* **640**, L119 (2006).
- [4] D. H. Rudd, A. R. Zentner, and A. V. Kravtsov, *The Astrophysical Journal* **672**, 19 (2008).
- [5] E. Semboloni, H. Hoekstra, J. Schaye, M. P. van Daalen, and I. G. McCarthy, *Monthly Notices of the Royal Astronomical Society* **417**, 2020 (2011).
- [6] J. Schaye, R. Kugel, M. Schaller, J. C. Helly, J. Braspennig, W. Elbers, I. G. McCarthy, M. P. Van Daalen, B. Vandenbroucke, C. S. Frenk, *et al.*, *Monthly Notices of the Royal Astronomical Society* **526**, 4978 (2023).
- [7] Ž. Ivezić, S. M. Kahn, J. A. Tyson, B. Abel, E. Acosta, R. Allsman, D. Alonso, Y. AlSayyad, S. F. Anderson, J. Andrew, *et al.*, *The Astrophysical Journal* **873**, 111 (2019).
- [8] J. Yao, H. Shan, R. Li, Y. Xu, D. Fan, D. Liu, P. Zhang, Y. Yu, C. Wei, B. Hu, *et al.*, *Monthly Notices of the Royal Astronomical Society* **527**, 5206 (2024).
- [9] A. M. Le Brun, I. G. McCarthy, J. Schaye, and T. J. Ponman, *Monthly Notices of the Royal Astronomical Society* **441**, 1270 (2014).
- [10] D. Nelson, A. Pillepich, S. Genel, M. Vogelsberger, V. Springel, P. Torrey, V. Rodriguez-Gomez, D. Sijacki, G. F. Snyder, B. Griffen, *et al.*, *Astronomy and Computing* **13**, 12 (2015).
- [11] J. Schaye, R. A. Crain, R. G. Bower, M. Furlong, M. Schaller, T. Theuns, C. Dalla Vecchia, C. S. Frenk, I. McCarthy, J. C. Helly, *et al.*, *Monthly Notices of the Royal Astronomical Society* **446**, 521 (2015).
- [12] I. G. McCarthy, J. Schaye, S. Bird, and A. M. C. Le Brun, *Monthly Notices of the Royal Astronomical Society*, stw2792 (2016).
- [13] D. Nelson, V. Springel, A. Pillepich, V. Rodriguez-Gomez, P. Torrey, S. Genel, M. Vogelsberger, R. Pakmor, F. Marinacci, R. Weinberger, *et al.*, *Computational Astrophysics and Cosmology* **6**, 2 (2019).
- [14] R. Pakmor, V. Springel, J. P. Coles, T. Guillet, C. Pfrommer, S. Bose, M. Barrera, A. M. Delgado, F. Ferlito, C. Frenk, *et al.*, *Monthly Notices of the Royal Astronomical Society* **524**, 2539 (2023).
- [15] J. Salcido, I. G. McCarthy, J. Kwan, A. Upadhye, and A. S. Font, *Monthly Notices of the Royal Astronomical Society* **523**, 2247 (2023).
- [16] J. Schaye, E. Chaikin, M. Schaller, S. Ploeckinger, F. Huško, R. McGibbon, J. W. Trayford, A. Benítez-Llambay, C. Correa, C. S. Frenk, *et al.*, arXiv preprint arXiv:2508.21126 (2025).
- [17] D. Sharma, B. Dai, F. Villaescusa-Navarro, and U. Seljak, *Monthly Notices of the Royal Astronomical Society* **538**, 1415 (2025).
- [18] L. Bigwood, M. Yamamoto, J. Siegel, A. Amon, I. G. McCarthy, R. Dave, J. Salcido, M. Schaller, J. Schaye, and T. Yang, arXiv preprint arXiv:2510.15822 (2025).
- [19] B. Hadzhiyska, S. Ferraro, B. R. Guachalla, E. Schaan, J. Aguilar, N. Battaglia, J. Bond, D. Brooks, E. Calabrese, S. Choi, *et al.*, arXiv preprint arXiv:2407.07152 (2024).
- [20] P. Popesso, A. Biviano, I. Marini, K. Dolag, S. Vladutescu-Zopp, B. Csizi, V. Biffi, G. Lamer, A. Robothan, M. Bravo, *et al.*, arXiv preprint arXiv:2411.16555 (2024).
- [21] J. Siegel, A. Amon, I. G. McCarthy, L. Bigwood, M. Yamamoto, E. Bulbul, J. E. Greene, J. McCullough, M. Schaller, and J. Schaye, arXiv preprint arXiv:2509.10455 (2025).
- [22] A. Schneider and R. Teyssier, *Journal of Cosmology and Astroparticle Physics* **2015** (12), 049.
- [23] M. Zennaro, G. Aricò, C. García-García, R. E. Angulo, L. Ondaro-Mallea, S. Contreras, A. Nicola, M. Schaller, and J. Schaye, arXiv preprint arXiv:2412.08623 (2024).
- [24] A. Wayland, D. Alonso, and M. Zennaro, *Monthly Notices of the Royal Astronomical Society* **543**, 1518 (2025).
- [25] B. Dai, Y. Feng, and U. Seljak, *Journal of Cosmology and Astroparticle Physics* **2018** (11), 009.
- [26] Z. Chen, P. Zhang, and X. Yang, *The Astrophysical Journal* **953**, 188 (2023).
- [27] B. R. Guachalla, E. Schaan, B. Hadzhiyska, S. Ferraro, J. N. Aguilar, S. Ahlen, N. Battaglia, D. Bianchi, R. Bond, D. Brooks, *et al.*, arXiv preprint arXiv:2503.19870 (2025).
- [28] T. Ferreira, D. Alonso, C. Garcia-Garcia, and N. E. Chisari, *Physical Review Letters* **133**, 051001 (2024).
- [29] E. Bulbul, A. Liu, M. Kluge, X. Zhang, J. Sanders, Y. Bahar, V. Ghirardini, E. Artis, R. Seppi, C. Garrel, *et al.*, *Astronomy & Astrophysics* **685**, A106 (2024).
- [30] J. M. Shull, B. D. Smith, and C. W. Danforth, *The Astrophysical Journal* **759**, 23 (2012).
- [31] M. McQuinn, *The Astrophysical Journal Letters* **780**,

- L33 (2013).
- [32] F. Nicastro, J. Kaastra, Y. Krongold, S. Borgani, E. Branchini, R. Cen, M. Dadina, C. Danforth, M. Elvis, F. Fiore, *et al.*, *Nature* **558**, 406 (2018).
- [33] J.-P. Macquart, J. Prochaska, M. McQuinn, K. Bannister, S. Bhandari, C. Day, A. Deller, R. Ekers, C. James, L. Marnoch, *et al.*, *Nature* **581**, 391 (2020).
- [34] S. Driver, *Nature Astronomy* **5**, 852 (2021).
- [35] L. Connor, V. Ravi, K. Sharma, S. K. Ocker, J. Faber, G. Hallinan, C. Harnach, G. Hellbourg, R. Hobbs, D. Hodge, *et al.*, *Nature Astronomy*, 1 (2025).
- [36] S. Zhou and P. Zhang, arXiv preprint arXiv:2510.11022 (2025).
- [37] M. Fukugita and P. J. E. Peebles, *The Astrophysical Journal* **616**, 643 (2004).
- [38] S. Cheng, Y.-S. Ting, B. Ménard, and J. Bruna, *Monthly Notices of the Royal Astronomical Society* **499**, 5902 (2020).
- [39] V. Springel, R. Pakmor, A. Pillepich, R. Weinberger, D. Nelson, L. Hernquist, M. Vogelsberger, S. Genel, P. Torrey, F. Marinacci, and J. Naiman, *Monthly Notices of the Royal Astronomical Society* **475**, 676 (2017).
- [40] D. Nelson, A. Pillepich, V. Springel, R. Weinberger, L. Hernquist, R. Pakmor, S. Genel, P. Torrey, M. Vogelsberger, G. Kauffmann, F. Marinacci, and J. Naiman, *Monthly Notices of the Royal Astronomical Society* **475**, 624 (2017).
- [41] A. Pillepich, D. Nelson, L. Hernquist, V. Springel, R. Pakmor, P. Torrey, R. Weinberger, S. Genel, J. P. Naiman, F. Marinacci, and M. Vogelsberger, *Monthly Notices of the Royal Astronomical Society* **475**, 648 (2017).
- [42] J. P. Naiman, A. Pillepich, V. Springel, E. Ramirez-Ruiz, P. Torrey, M. Vogelsberger, R. Pakmor, D. Nelson, F. Marinacci, L. Hernquist, R. Weinberger, and S. Genel, *Monthly Notices of the Royal Astronomical Society* **477**, 1206 (2018).
- [43] F. Marinacci, M. Vogelsberger, R. Pakmor, P. Torrey, V. Springel, L. Hernquist, D. Nelson, R. Weinberger, A. Pillepich, J. Naiman, and S. Genel, *Monthly Notices of the Royal Astronomical Society* 10.1093/mnras/sty2206 (2018).
- [44] M. Vogelsberger, S. Genel, V. Springel, P. Torrey, D. Sijacki, D. Xu, G. Snyder, S. Bird, D. Nelson, and L. Hernquist, *Nature* **509**, 177 (2014).
- [45] M. Vogelsberger, S. Genel, V. Springel, P. Torrey, D. Sijacki, D. Xu, G. Snyder, D. Nelson, and L. Hernquist, *Monthly Notices of the Royal Astronomical Society* **444**, 1518 (2014).
- [46] S. Genel, M. Vogelsberger, V. Springel, D. Sijacki, D. Nelson, G. Snyder, V. Rodriguez-Gomez, P. Torrey, and L. Hernquist, *Monthly Notices of the Royal Astronomical Society* **445**, 175 (2014).
- [47] D. Sijacki, M. Vogelsberger, S. Genel, V. Springel, P. Torrey, G. F. Snyder, D. Nelson, and L. Hernquist, *Monthly Notices of the Royal Astronomical Society* **452**, 575 (2015).
- [48] S. Mallat, *Communications on Pure and Applied Mathematics* **65**, 1331 (2012).
- [49] J. Bruna and S. Mallat, *IEEE transactions on pattern analysis and machine intelligence* **35**, 1872 (2013).
- [50] M. Eickenberg, G. Exarchakis, M. Hirn, S. Mallat, and L. Thiry, *The Journal of chemical physics* **148** (2018).
- [51] A. Taylor, Arxiv preprint astro-ph/0111605 (2001).
- [52] W. Hu and C. R. Keeton, *Physical Review D* **66**, 063506 (2002).
- [53] D. Bacon and A. Taylor, *Monthly Notices of the Royal Astronomical Society* **344**, 1307 (2003).
- [54] N. Aghanim *et al.*, *Astron. Astrophys* **641**, A6 (2020).
- [55] T. Louis, A. La Posta, Z. Atkins, H. T. Jense, I. Abril-Cabezas, G. E. Addison, P. A. Ade, S. Aiola, T. Alford, D. Alonso, *et al.*, arXiv preprint arXiv:2503.14452 (2025).
- [56] S. Alam, M. Aubert, S. Avila, C. Balland, J. E. Bautista, M. A. Bershad, D. Bizyaev, M. R. Blanton, A. S. Bolton, J. Bovy, *et al.*, *Physical Review D* **103**, 083533 (2021).
- [57] M. A. Karim, J. Aguilar, S. Ahlen, S. Alam, L. Allen, C. Allende Prieto, O. Alves, A. Anand, U. Andrade, E. Armengaud, *et al.*, arXiv e-prints, arXiv (2025).
- [58] A. Adame, J. Aguilar, S. Ahlen, S. Alam, G. Aldering, D. Alexander, R. Alfarsy, C. A. Prieto, M. Alvarez, O. Alves, *et al.*, *The Astronomical Journal* **167**, 62 (2024).
- [59] C. Zhao, S. Huang, M. He, P. Montero-Camacho, Y. Liu, P. Renard, Y. Tang, A. Verdier, W. Xu, X. Yang, *et al.*, arXiv preprint arXiv:2411.07970 (2024).
- [60] B. Zhang, *Reviews of Modern Physics* **95**, 035005 (2023).
- [61] C. Leung, J. Borrow, K. W. Masui, S. Andrew, K.-F. Chen, J. Schaye, and M. Schaller, arXiv preprint arXiv:2509.19514 (2025).
- [62] A. Fialkov and A. Loeb, *The Astrophysical Journal Letters* **846**, L27 (2017).
- [63] G. Hallinan, V. Ravi, S. Weinreb, J. Kocz, Y. Huang, D. Woody, J. Lamb, L. D'Addario, M. Catha, J. Shi, *et al.*, arXiv preprint arXiv:1907.07648 (2019).
- [64] H.-H. Lin, K.-y. Lin, C.-T. Li, Y.-H. Tseng, H. Jiang, J.-H. Wang, J.-C. Cheng, U.-L. Pen, M.-T. Chen, P. Chen, *et al.*, *Publications of the Astronomical Society of the Pacific* **134**, 094106 (2022).
- [65] Z. Vlah, E. Castorina, and M. White, *Journal of Cosmology and Astroparticle Physics* **2016** (12), 007.
- [66] Z. Vlah, U. Seljak, and T. Baldauf, *Physical Review D* **91**, 023508 (2015).
- [67] M. White, *Monthly Notices of the Royal Astronomical Society* **439**, 3630 (2014).
- [68] N. Kokron, S.-F. Chen, M. White, J. DeRose, and M. Maus, *Journal of Cosmology and Astroparticle Physics* **2022** (09), 059.
- [69] S.-F. Chen, Z. Vlah, and M. White, *Journal of Cosmology and Astroparticle Physics* **2020** (07), 062.
- [70] S. Zhou, Z. Chen, and Y. Yu, *Science China Physics, Mechanics & Astronomy* **68**, 1 (2025).
- [71] G. Bruzual and S. Charlot, *Monthly Notices of the Royal Astronomical Society* **344**, 1000 (2003).
- [72] G. Kauffmann, T. M. Heckman, S. D. White, S. Charlot, C. Tremonti, J. Brinchmann, G. Bruzual, E. W. Peng, M. Seibert, M. Bernardi, *et al.*, *Monthly Notices of the Royal Astronomical Society* **341**, 33 (2003).
- [73] Y. Zu and R. Mandelbaum, *Monthly Notices of the Royal Astronomical Society* **454**, 1161 (2015).
- [74] R. Battye, I. Browne, C. Dickinson, G. Heron, B. Maffei, and A. Pourtsidou, *Monthly Notices of the Royal Astronomical Society* **434**, 1239 (2013).
- [75] P. Bull, P. G. Ferreira, P. Patel, and M. G. Santos, *The Astrophysical Journal* **803**, 21 (2015).

Baryonic effects on structure growth: analysis with Zel'dovich approximation

Assumption (I) states that baryonic feedback predominantly affects the amplitude rather than the phase of the matter field. This behavior is verified by measurements in TNG300-1 and Illustris-1 simulations (Fig. 1), and further supported by Ref. [17], which reaches the same conclusion based on thousands of hydrodynamical simulations. A physical intuition is embedded in the contrast between the suppressed amplitude and yet tight cross-correlation with the DMO counterpart. At a fixed scale, baryonic effects can suppress the clustering strength, but struggle to disrupt the overall similarity of structures between two universes. Consequently, the sensitivity of matter clustering to baryonic effects is much larger in the amplitude, quantified by $\sqrt{P_{mm}/P_{\text{DMO}}}$, than in the phase, the structural similarity quantified by $r(\delta_m, \delta_{\text{DMO}})$. Beyond numerical verification, we can gain more physical intuition from the framework of large-scale structure perturbation theory.

In Lagrangian perturbation theory, a fluid element initially located at position \mathbf{q} at redshift z_0 evolves dynamically to the Eulerian position $\mathbf{x}(\mathbf{q}, z) = \mathbf{q} + \Psi(\mathbf{q}, z)$, where $\mathbf{q} = \mathbf{x}(\mathbf{q}, z_0)$. Hereafter, we use redshift z as the time variable. The mass conversation yields

$$1 + \delta_m(\mathbf{x}, z) = \int_{\mathbf{q}} [1 + \delta(\mathbf{q})] \delta^D(\mathbf{x} - \mathbf{q} - \Psi(\mathbf{q}, z)) , \quad (8)$$

where $\int_{\mathbf{q}} \dots \equiv \int d^3\mathbf{q} \dots$ denotes the integral over Lagrangian space. The displacement field $\Psi(\mathbf{q}, z)$ maps the matter overdensity from the Lagrangian space $\delta(\mathbf{q})$ to the Eulerian space $\delta_m(\mathbf{x}, z)$ at redshift z , where $\delta(\mathbf{q}) \equiv \delta_m(\mathbf{q}, z_0)$. The matter power spectrum in a DMO universe is therefore given by

$$(2\pi)^3 \delta_{k,0}^D + P_{mm}(k, z) = \int_{\mathbf{q}} e^{-i\mathbf{k}\cdot\mathbf{q}} \langle [1 + \delta(\mathbf{q}_1)][1 + \delta(\mathbf{q}_2)] e^{i\mathbf{k}\cdot\Delta} \rangle . \quad (9)$$

where $\Delta = \Psi(\mathbf{q}_1, z) - \Psi(\mathbf{q}_2, z)$, and Ψ is the displacement solely induced by gravity. For simplicity, we adopt the Zel'dovich approximation $\Psi(\mathbf{k}) \simeq \Psi^Z(\mathbf{k}) = i\mathbf{k} k^{-2} \delta(\mathbf{k})$ and further assume that $\delta(\mathbf{q})$ is a Gaussian field. The matter power spectrum with $k \neq 0$ is therefore simplified to [65–69]

$$P_{zz}(k) = \int_{\mathbf{q}} e^{-i\mathbf{k}\cdot\mathbf{q}} e^{-\frac{1}{2}\langle\Delta\Delta\rangle_c} [1 + i\langle(\delta_1 + \delta_2)\Delta\rangle_c + \langle\delta_1\delta_2\rangle_c - \langle\delta_1\Delta\rangle_c\langle\delta_2\Delta\rangle_c] . \quad (10)$$

Here $\delta_i \equiv \delta(\mathbf{q}_i)$, $\Delta \equiv \mathbf{k} \cdot \Delta$, and $\langle \dots \rangle_c$ is the cumulant of stochastic fields.

The primary impacts on matter clustering of baryonic effects, including gas cooling, star formation, and AGN feedback, are complex but highly local. These processes mainly alter the internal structures of halos, for instance by expanding or redistributing matter within them, rather than directly modifying large-scale perturbations. Consequently, during the coevolution of baryons and cold dark matter, baryonic effects can be regarded as an additional short-range force acting on the matter motion relative to its DMO counterpart. In the Lagrangian framework, this short-range force from baryons induces an extra displacement field Ψ_s , which dominates small-scale structure formation but remains subdominant to gravity on large scales, satisfying $|\Psi_s(\mathbf{k})| \ll |\Psi(\mathbf{k})|$ for $|\mathbf{k}| \ll R_b^{-1}$, where $R_b \sim 1$ Mpc characterizes the scale below which baryonic physics are significant. By substituting $\Psi \rightarrow \Psi + \Psi_s$ into Eq. (8) & Eq. (9), we obtain the modified matter overdensity field and matter power spectrum in the presence of baryons.

We consider a scenario in which the universe evolves purely under gravity until redshift z . Starting from z and lasting for a short duration $\Delta z \ll 1$, baryonic processes induce an additional displacement Ψ_s . The matter overdensity field with this baryonic shift is

$$1 + \delta_s(\mathbf{x}, z + \Delta z) = \int_{\mathbf{q}} [1 + \delta(\mathbf{q}; z)] \delta^D(\mathbf{x} - \mathbf{q} - \Psi(\mathbf{q}, z + \Delta z; z) - \Psi_s(\mathbf{q}, z + \Delta z; z)) , \quad (11)$$

where $\Psi(\mathbf{q}, z + \Delta z; z) = \Psi(\mathbf{q}, z + \Delta z) - \Psi(\mathbf{q}, z)$. By adopting the Zel'dovich approximation as in Eq. (10), the power spectrum of δ_s is obtained

$$P_{ss}(k) = \int_{\mathbf{q}} e^{-i\mathbf{k}\cdot\mathbf{q}} e^{-\frac{1}{2}\langle(\Delta+\Delta_s)^2\rangle_c} [1 + i\langle(\delta_1 + \delta_2)(\Delta + \Delta_s)\rangle_c + \langle\delta_1\delta_2\rangle_c - \langle\delta_1(\Delta + \Delta_s)\rangle_c\langle\delta_2(\Delta + \Delta_s)\rangle_c] \quad (12)$$

$$= \int_{\mathbf{q}} e^{-i\mathbf{k}\cdot\mathbf{q}} e^{-\frac{1}{2}\langle\Delta\Delta\rangle_c} [1 + i\langle(\delta_1 + \delta_2)\Delta\rangle_c + \langle\delta_1\delta_2\rangle_c - \langle\delta_1\Delta\rangle_c\langle\delta_2\Delta\rangle_c - \langle\Delta\Delta_s\rangle + i\langle(\delta_1 + \delta_2)\Delta_s\rangle_c - \langle\delta_1\Delta\rangle_c\langle\delta_2\Delta_s\rangle_c - \langle\delta_1\Delta_s\rangle_c\langle\delta_2\Delta\rangle_c + \mathcal{O}(k^2\Psi_s^2)] \quad (13)$$

$$= P_{zz}(k) + I_s(k) + \mathcal{O}(k^2\Psi_s^2) , \quad (14)$$

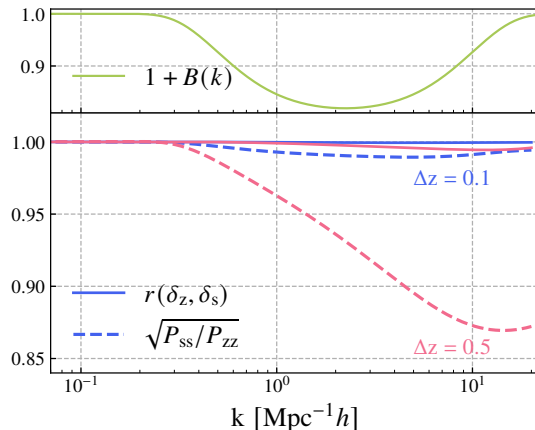


FIG. 4. Baryonic effects on the matter power spectrum modeled with the Zel'dovich approximation. We model the baryonic effect as an additional displacement $\Psi_s(\mathbf{k}) = B(k)\Psi^Z(\mathbf{k})$, where the window function is given by $B(k) = \alpha e^{-(k_l/k)^2 - (k/k_s)^2}$, with $\alpha = -0.2$, $k_l = 0.5 h/\text{Mpc}$ and $k_s = 10 h/\text{Mpc}$. The small-scale power is further damped by a factor $e^{-(k/k_s)^2}$ to localize the Ψ_s impacts in Fourier space. We perform calculations that evolve the DMO density field from $z = 1$ to $z + \Delta z$ with/without the baryonic shift Ψ_s , for two cases: $\Delta z = 0.1$ (blue) and $\Delta z = 0.5$ (red). *Top panel*: The adopted window function $B(k)$. *Bottom panel*: The resulted baryonic suppression of the matter power spectrum (*dashed*) and cross-correlation coefficients between δ_s and δ_z (*solid*). The results verify the conclusion that the matter clustering is sensitive to baryonic effects in amplitude than in phase under the Zel'dovich approximation.

where $\Delta_s = \mathbf{k} \cdot [\Psi_s(\mathbf{q}_1) - \Psi_s(\mathbf{q}_2)]$ and the baryon contribution in P_{ss} is

$$I_s(k) = \int_{\mathbf{q}} e^{-i\mathbf{k}\cdot\mathbf{q}} e^{-\frac{1}{2}\langle\Delta\Delta\rangle_c} [-\langle\Delta\Delta_s\rangle + i\langle(\delta_1 + \delta_2)\Delta_s\rangle_c - \langle\delta_1\Delta\rangle_c\langle\delta_2\Delta_s\rangle_c - \langle\delta_1\Delta_s\rangle_c\langle\delta_2\Delta\rangle_c]. \quad (15)$$

Similarly, the cross power spectrum between δ_z and δ_s is

$$P_{zs}(k) = P_{zz}(k) + \frac{1}{2}I_s(k) + \mathcal{O}(k^2\Psi_s^2). \quad (16)$$

Power spectra P_{ss} , P_{zz} , and P_{zs} denote the matter power spectrum with baryonic effects, its DMO counterpart, and their cross-correlation, respectively. Hence, the cross-correlation coefficient between δ_z and δ_s is

$$r_{zs}(k) \equiv \frac{P_{zs}(k)}{\sqrt{P_{zz}(k)P_{ss}(k)}} \simeq 1 + \mathcal{O}\left(\frac{\Psi_s^2}{\Psi^2}\right), \quad (17)$$

Here $\Psi = |\Psi|$, $\Psi_s = |\Psi_s|$ and $\Psi_s/\Psi \ll 1$ on large scales. The suppression of the matter power spectrum resulting from the baryonic shift is

$$S(k) \equiv \sqrt{\frac{P_{ss}(k)}{P_{zz}(k)}} = 1 + \frac{1}{2}\frac{I_s(k)}{P_{zz}(k)} + \mathcal{O}\left(\frac{\Psi_s^2}{\Psi^2}\right) \simeq 1 + \mathcal{O}\left(\frac{\Psi_s}{\Psi}\right). \quad (18)$$

where $I_s(k) \sim \mathcal{O}(k\Psi_s)$. In this scenario, the leading-order contribution of baryonic effects to the cross-correlation coefficient r_{zs}^2 is canceled, resulting in deviations from unity only at the order $\sim (\Psi_s/\Psi)^2$. In contrast, the matter power spectrum is suppressed by a proportion $I_s/P_{zz} \sim \Psi_s/\Psi$, which is larger by one order of magnitude. In this case, we demonstrate that the matter clustering is an order-of-magnitude more sensitive to baryonic effects in amplitude than in phase.

We further perform direct integrations of Eq. (10), Eq. (12) & Eq. (16), with full resummation of δ , Ψ and Ψ_s correlators, without assuming an evolution over an infinitesimal time step. For simplicity, we assume that Ψ_s is proportional to the gradient of the potential, i.e., $\Psi_s(\mathbf{k}, z) = B(k)\frac{i\mathbf{k}}{k^2}\delta(\mathbf{k}, z)$, following a form similar to the model for correcting simulation resolution effects in Ref. [25]. The window function $B(k)$ is chosen to (i) be negative, mimicking the resistant force such as gas pressure that counteracts halo collapse; (ii) be dominated by small-scale power, as baryonic feedback predominantly affects small-scale structure. In Fig. 4, we show the results obtained using this toy

model to calculate the baryonic suppression $S(k)$ and the cross-correlation r_{zs} , by evolving the DMO density field from $z = 1$ to $z + \Delta z$. The numerical implementation follows the same strategy in Ref. [70], which modifies the code from Ref. [69], and all input linear power spectra are smoothed by $e^{-(k/50)^2}$ to cut the small-scale power. Although the adopted Ψ_s model is highly simplified, it reproduces the behavior found in hydrodynamical simulations and is consistent with the previous order-of-magnitude analysis, that the baryonic effects impact the amplitude of matter clustering roughly an order of magnitude more strongly than the phase. The agreement between these numerical integrations and the hydrodynamical simulations also supports the validity of the assumed behavior of Ψ_s described above. In principle, one could include non-linear and stochastic effects to construct a more realistic model of the displacement induced by baryons, beyond this toy model that merely attenuates the gravitational displacement, but their overall behavior nevertheless remains described by Eq. (17) and Eq. (18).

Baryon tracers and tomographic measurements

We decompose the total baryon overdensity δ_b into three contributions: the free ionized electrons δ_e traced by the dispersion measure of FRBs, the clustering of stellar content δ_* estimated from galaxy surveys, and the neutral hydrogen δ_{HI} traced by the 21cm lines mapping. The validity of this implementation is trivial, as it is merely a classification of major baryons, while unaccounted components such as metals contribute negligibly to total baryon content.

To deproject the mixed Fourier modes, we utilize galaxy samples with a narrow redshift width $\Delta z_g \ll 1$ centered at a comoving distance χ_g , e.g., $\Delta z = 0.1$ as in Ref. [36]. The Limber approximation leads to $C_\ell^{gX} = \chi_g^{-2} W_X(\chi_g) P_{gi}(\ell/\chi_g, z)$, and the expectation of Eq. (7) becomes

$$\langle \widehat{f_i b_i}(\ell) \rangle = \mathcal{A}_i \frac{W_{X_i}(\chi_g) P_{gi}(k)}{W_\kappa(\chi_g) P_{gm}(k)} \Big|_{\ell=k\chi_g} = f_i b_i(k). \quad (19)$$

In this limit, each Fourier mode is directly measurable. The kernel function of weak lensing is $W_\kappa(\chi) = \frac{3}{2c^2} \Omega_{m0} H_0^2 a^{-1} \chi N_\kappa(z)$, where $N_\kappa(z) = \int_z^\infty dz_s n_s(z_s) (1 - \chi/\chi_s)$ is redshift distribution integral of lensing source $n_s(z_s)$. The scalar amplitude $\mathcal{A}_i \equiv f_i W_\kappa(\chi_g)/W_{X_i}(\chi_g)$ only relies on cosmological parameters, because of $W_{X_i} \propto f_i$ for three baryon tracers, as specified below.

The primary baryon tracer is FRB, as it directly probes free electrons in ionized diffuse gas through dispersion measure [60],

$$\mathcal{D} = \frac{3H_0^2 \Omega_{b0}}{8\pi G m_p} \int d\chi a^{-1} f_e (1 + \delta_e). \quad (20)$$

Here, the backlight of FRBs traces the electron density fluctuation δ_e projected along the radial distance χ . In the tomographic measurement using galaxy samples with a narrow redshift distribution, we have

$$\mathcal{A}_e = \frac{4\pi G m_p \Omega_{m0}}{c^2 \Omega_{b0}} \chi_g \frac{N_\kappa(z_g)}{N_{\mathcal{D}}(z_g)} \quad (21)$$

where $N_{\mathcal{D}}(z) = \int_z^\infty dz_s n_{\mathcal{D}}(z_s)$ is the redshift distribution integral $n_{\mathcal{D}}(z_s)$ of FRBs. The clustering of stellar content and neutral hydrogen are two subdominant contributions to the total baryon clustering. Given the stellar evolution prescription, the stellar mass M_* is estimated by observables such as photometries and spectral characteristics [71–73]. We can therefore measure the stellar surface density by $\hat{\Sigma}_*(\hat{n}_{\text{pix}}) = \Delta\Omega^{-1} \sum_{\hat{n} \in \text{pix}} M_*(\hat{n})$ in form, where $\Delta\Omega$ is the angular area of the pixel. Here, we neglect the finite extent of galaxies since the typical value of galaxy size is much smaller than the minimum scale ~ 1 Mpc we are interested in. The expectation of the estimate after survey systematics correction is

$$\Sigma_* = \frac{3cH_0^2}{8\pi G} \Omega_{b0} \frac{\chi^2}{H(z)} \Delta z_g f_* (1 + \delta_*) , \quad (22)$$

where Δz_g is the projected depth of stellar samples, chosen to be the same as galaxy clustering with $\Delta z_g \ll 1$ and leading to

$$\mathcal{A}_* = \frac{4\pi G \Omega_{m0}}{c^2 \Omega_{b0}} \frac{1+z}{\chi_g} \frac{N_\kappa(z_g)}{\Delta z_g^{-1}}. \quad (23)$$

For neutral hydrogen, they are traced by the surface brightness temperature of 21cm lines [74, 75],

$$T_b = \frac{9}{128\pi} \frac{\hbar c^3 A_{10}}{k_B \nu_{21}^2 G m_p} \frac{H_0^2 (1+z)^2}{H(z)} \Omega_{b0} f_{\text{HI}} (1 + \delta_{\text{HI}}) . \quad (24)$$

It gives

$$\mathcal{A}_{\text{HI}} = \frac{64\pi}{3} \frac{k_B \nu_{21}^2 G m_p}{\hbar c^4 A_{10}} \frac{\Omega_{m0}}{\Omega_{b0}} \frac{\chi_g}{1+z} \frac{N_\kappa(z_g)}{N_{\text{HI}}(z_g)} , \quad (25)$$

where we choose the redshift distribution of 21cm sources as narrow as galaxies to maximize the detection significance, i.e., $N_{\text{HI}}(z) \simeq \Delta z_g^{-1}$. The explicit expressions of \mathcal{A}_e , \mathcal{A}_* and \mathcal{A}_{HI} in Eqs. (21, 21, 25) demonstrates that the estimations of these overall factors \mathcal{A}_i are independent of astrophysics, only relying on the cosmological parameters that are tightly constrained by the CMB and BAO observations.

The solution for baryonic effects shares the same philosophy as the cosmological Cavendish experiment proposed in Ref. [36], though the two are distinguished by their different objectives. The Cavendish experiment focuses on linear perturbation, where the number of modes is limited. Thus, the precision of gravitational constant measurement is about $\sim 10\%$ with 10^5 FRBs, making the corrections from $f_* b_*$ and $f_{\text{HI}} b_{\text{HI}}$ subdominant relative to the statistical uncertainties. In contrast, to correct the baryonic feedback, forthcoming surveys demand systematic corrections better than 1% accuracy across a wide range of scales $k \sim 0.01 - 1 h/\text{Mpc}$. The minor mitigations from $f_* b_*$ and $f_{\text{HI}} b_{\text{HI}}$ become non-negligible.

Auxiliary results of simulation measurements

In Fig. 5, we compare the baryonic suppression $\mathcal{T}^{-1}(k) = \sqrt{P_{mm}(k)/P_{\text{DMO}}(k)}$ and the cross-correlation coefficients $r(\delta_m, \delta_{\text{DMO}})$ measured in simulations. The aggressive AGN feedback employed in the Illustris-1 simulation significantly modifies the matter distribution, resulting in a strong suppression of the matter power spectrum compared to its DMO counterparts. In contrast, the baryonic effects in TNG300-1 are mild.

In Fig. 6, we present $\{f_e b_e, f_* b_*, f_{\text{HI}} b_{\text{HI}}\}$ that directly measured in TNG300-1 and Illustris-1 simulations. In Fig. 7, we present three variants of \mathcal{T} estimate by excluding $f_* b_*$, $f_{\text{HI}} b_{\text{HI}}$ or both. These results verify that both stellar content and neutral hydrogen are subdominant contributions compared to ionized electrons, and their contributions to \mathcal{T} are roughly $\delta\mathcal{T}_* + \delta\mathcal{T}_{\text{HI}} \sim \Omega_b/\Omega_c (f_* b_* + (1+\eta)f_{\text{HI}} b_{\text{HI}}) \sim 0.01$. The specific fractions depend on simulation details, with $\sim 1.5\%$ for TNG300-1 and $\sim 3\%$ for Illustris-1. Nevertheless, the systematic shifts of both estimations are non-negligible in forthcoming shear measurement with $< 1\%$ precision.

A direct consequence of assumption **(I)**, as also indicated by Eq. (1), is that \mathcal{T} removes baryonic feedback from matter clustering at the field level [17], rather than merely at the power-spectrum level. Consequently, baryonic effects are also eliminated from all summarized statistics. The accuracy of this removal is primarily governed by the validity of Eq. (4), where our results suggest holds to within $k \lesssim 1 h/\text{Mpc}$. In the main text, we take the scattering transform coefficient as an example. The scattering transform of the input field $I_0(\mathbf{x})$ is defined as

$$\begin{aligned} I_{jl}(\mathbf{x}) &= |I_0 * \psi_{jl}|(\mathbf{x}) , \\ I_{j_1 l_1; j_2 l_2}(\mathbf{x}) &= |I_{j_1 l_1} * \psi_{j_2 l_2}|(\mathbf{x}) , \\ &\dots , \end{aligned}$$

where $*$ denotes the convolution operator, and the modulo operator $|...|$ introduces the non-linearity to extract the higher-order correlations. The scattering coefficients of the stochastic field are defined as

$$\begin{aligned} S_0 &= \langle I_0 \rangle_{\mathbf{x}} , \\ S_{jl} &= \langle I_{jl} \rangle_{\mathbf{x}} = \langle |I_0 * \psi_{jl}| \rangle_{\mathbf{x}} , \\ S_{j_1 l_1; j_2 l_2} &= \langle I_{j_1 l_1; j_2 l_2} \rangle_{\mathbf{x}} = \langle |I_0 * \psi_{j_1 l_1}| * \psi_{j_2 l_2} | \rangle_{\mathbf{x}} , \\ &\dots , \end{aligned}$$

where $\langle \dots \rangle_{\mathbf{x}}$ denotes averaging over all pixels in real space. For simplicity, we present the results of S_{jl} and $S_{j_1 l_1; j_2 l_2}$, and do not consider the mean of the input field S_0 and the higher order coefficients. We present the scattering coefficients for Illustris-1 simulation at $z = 0.5$ in Fig. 3, and show additional snapshots at $z = 0.0, 0.3, 0.7, 1.0$ in

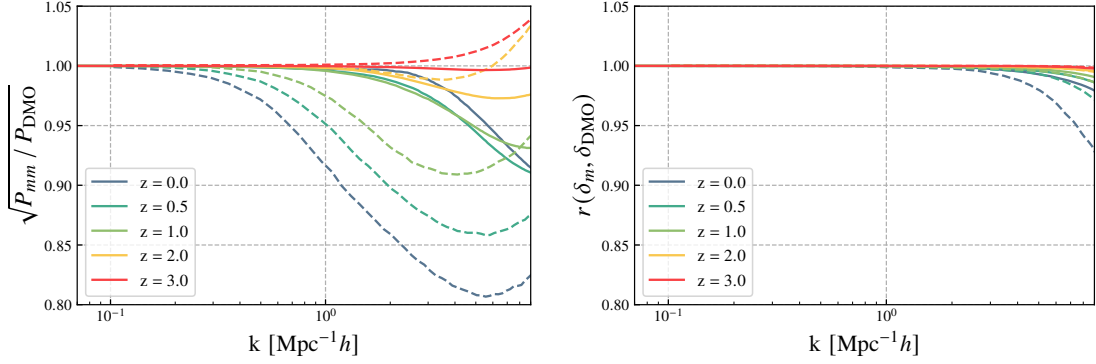


FIG. 5. Baryonic suppression (*left panel*) and cross-correlation coefficient (*right panel*) measured in TNG300-1 (*solid lines*) and Illustris-1 (*dashed lines*) simulations. Different colors correspond to different redshifts, covering the range $0 < z < 3$.

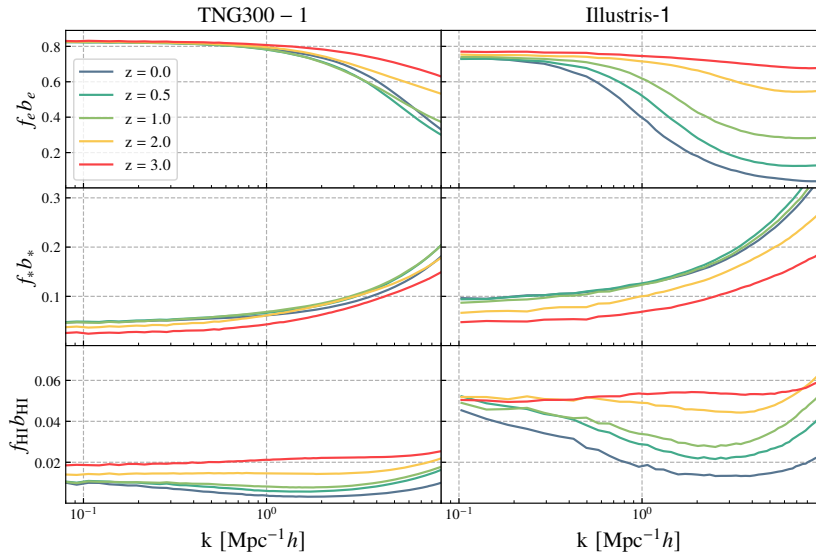


FIG. 6. Measurements of $f_i b_i$ in hydrodynamical simulation TNG300-1 (*left*) and Illustris-1 (*right*). From top to bottom panels, we show the measurement for free ionized electrons, star+black hole, and neutral hydrogen, respectively. Different colors correspond to different redshifts, covering the range $0 < z < 3$.

Fig. 8. Across $0 < z < 1$, baryonic feedback induces a suppression in the scattering coefficients, which is effectively removed by the transfer function $\hat{\mathcal{T}}$. The effectiveness of this correction depends on the $\hat{\mathcal{T}}$ accuracy. Because $\hat{\mathcal{T}}$ achieves higher accuracy at high redshift $z = 1$ than at low redshift $z = 0$ (Fig. 2), the scattering coefficients of the reconstructed field $\hat{\delta}_{\text{DMO}}(\mathbf{x}) = \hat{\mathcal{T}} * \delta_m(\mathbf{x})$ match the DMO counterpart within $\sim 1\%$ down to resolution $k_\sigma \simeq 5 h/\text{Mpc}$ at $z = 1$, compared to $k_\sigma \simeq 2.5 h/\text{Mpc}$ at $z = 0$. These results reinforce the conclusions in the main text.

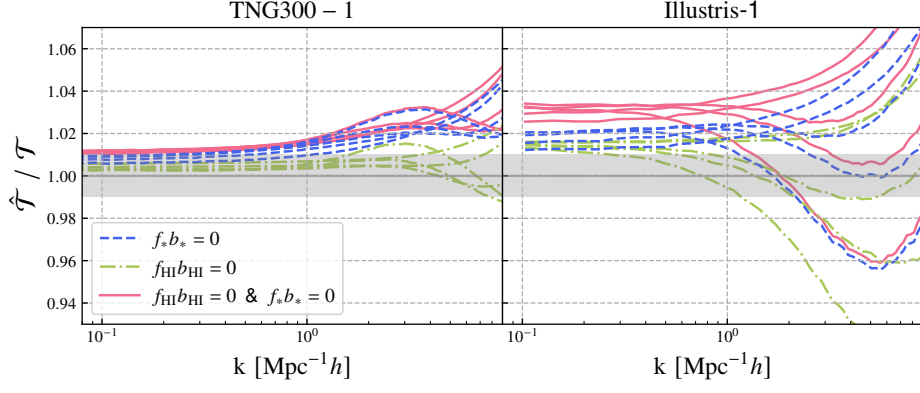


FIG. 7. Similar to Fig. 2, but we consider three variants of $\hat{\mathcal{T}}$: excluding $f_* b_*$ (blue, dashed), excluding $f_{\text{HI}} b_{\text{HI}}$ (green, dash-dotted), and excluding both $f_* b_*$ and $f_{\text{HI}} b_{\text{HI}}$ (red, solid). All 5 redshift bins are shown in the same colors.

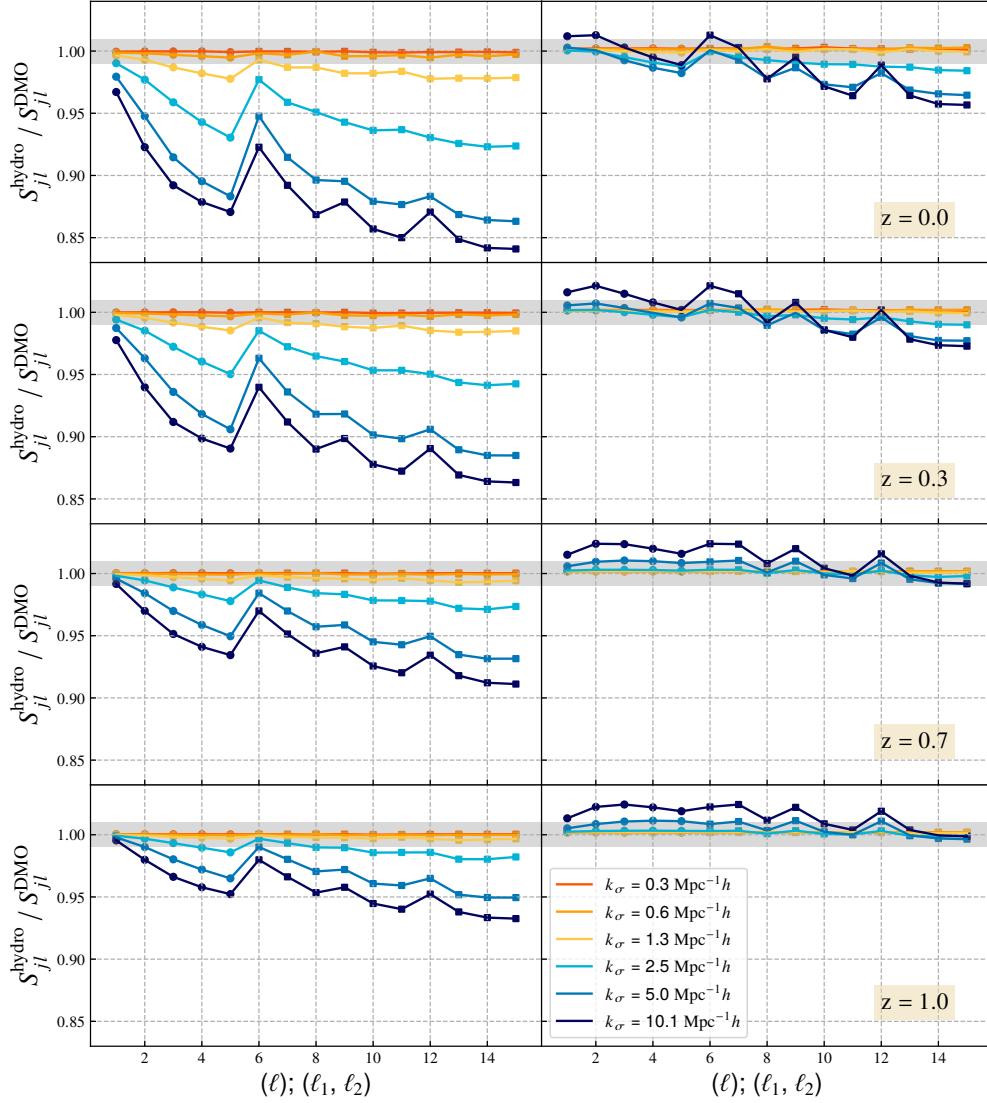


FIG. 8. Same as Fig. 3, but we present the results at $z = 0.0, 0.3, 0.7, 1.0$ redshift snapshots in Illustris-1 simulation from top to bottom panels, respectively.